

Safe platooning control of connected and autonomous vehicles on curved multi-lane roads

Xiao Chen¹, Zhiqi Tang¹, Karl H. Johansson¹ and Jonas Mårtensson¹

Abstract—This paper investigates the safe platoon formation tracking and merging control problem of connected and automated vehicles (CAVs) on curved multi-lane roads. The first novelty is the separation of the control designs into two distinct parts: a lateral control law that ensures a geometrical convergence towards the reference path regardless of the translational velocity, and a longitudinal control design for each vehicle to achieve the desired relative arc length and velocity with respect to its neighboring vehicle. The second novelty is exploiting the constructive barrier feedback as an additive term to the nominal tracking control, ensuring both lateral and longitudinal collision avoidance. This constructive barrier feedback acts as a dissipative term, slowing down the relative velocity toward obstacles without affecting the nominal controller’s performance. Consequently, our proposed control method enables safe platoon formation of vehicles on curved multi-lane roads, with theoretical guarantees for safety invariance and stability analysis. Simulation and experimental results on connected vehicles are provided to further validate the effectiveness of the proposed method.

I. INTRODUCTION

Interest in connected and automated vehicles (CAVs) has surged in recent years, driven by advancements in automation and communication technologies. CAVs offer the potential for cooperative on-road operations, promising significant benefits to the transportation sector. Vehicle platooning has emerged as a popular concept among the various forms of cooperative driving technology. Platooning involves a train of CAVs operating with minimal inter-vehicle distances and synchronized speeds. The exploration of vehicle platooning traces back to the early 2000s, initiated by pioneering projects such as PATH [1] and Sartre [2], which aimed to assess the potential benefits of this technology. Subsequent studies such as [3]–[5] have reinforced that vehicle platooning is promising to improve traffic efficiency, enhance safety, and reduce energy consumption.

Earlier works on designing control techniques to support vehicle platooning mainly focused on the simplified one-dimensional longitudinal control of vehicles for distance keeping and velocity synchronization by guaranteeing string stability through the design [6]–[8]. In a more general multi-lane traffic setting, multi-vehicle platooning requires adaptive formation adjustments of vehicles from different lanes while accommodating the road’s shape. The key challenge here is to design efficient platoon control strategies for multi-vehicle systems in structured road environments, preventing vehicle-to-vehicle collisions and encroachment on road boundaries.

Most of the existing work in the literature about safe platooning and merging control in multi-lane scenarios is restricted to the simplified type of roads with straight lines, and a majority of them typically focus only on lateral or longitude controller design. For instance, the work in [9] adopts potential function-based control strategies for a group of vehicles autonomously driving on the straight-line road with velocity consensus. Some other work uses optimization-based controllers, such as model predictive control and barrier function-based optimization controllers. In the work of [10], a safety-assuring MPC framework is developed, however, focusing only on safe lateral merging maneuvers of vehicles on straight-line roads. Another approach in [11] exploits barrier function-based optimization controllers but only for longitudinal merging control. It is worth noting that the use of optimization-based controllers poses challenges in explicitly analyzing the equilibrium and convergence of the multi-vehicle system, in addition to potential computational complexity and feasibility issues. To the best of our knowledge, the control problems of safe platooning and merging for CAVs on multi-laned and curved roads remain open.

Motivated by the above-mentioned open problems, in this paper, we propose a novel decentralized control strategy for the safe platooning and merging problem on curved multi-lane roads, covering both longitudinal and lateral design. Each vehicle is modeled as a nonholonomic second-order kinematic bicycle model. To handle the platoon formation tracking control on curved roads, we decouple the control design strategy into path following and formation control problems. Specifically, on one side, lateral control laws are designed for each vehicle ensuring a geometrical convergence towards the reference path regardless of the translational velocity; on the other side, longitudinal control laws are proposed for each vehicle to achieve the desired relative arc length and velocity with respect to its neighboring vehicle.

One of the key distinctions of the proposed work is that we adopt a novel concept of constructive barrier feedback, first presented in [12], for reactive collision avoidance. The constructive barrier feedback exploits *divergent flow* [13], a natural feature inspired by insects and birds, to prevent collisions while effectively achieving the primary control objective. In this work as well as in our preliminary work [14], constructive barrier feedback is exploited as an additive term to the nominal lateral and longitudinal controllers, which effectively avoids collision between neighboring vehicles and the road edges without compromising the nominal control objectives. Building on our preliminary results in

¹ Division of Decision and Control Systems, School of Electrical Engineering and Computer Science, KTH Royal Institute of Technology, Sweden. Emails: {xiao2, ztang2, kallej, jonas1}@kth.se

[14], which considered simplified vehicle dynamics (second-order systems) and straight roads, this work extends the previous findings by addressing a group of CAVs modeled as nonholonomic second-order kinematic bicycle systems operating on curved roads. The incorporation of constructive barrier feedback enables the design to take an explicit state-feedback form, offering a simple and elegant structure with low computational complexity, while providing formal guarantees for safety invariance and stability.

Under the proposed control methods, all vehicles accurately track the desired reference path and converge to the desired formation while maintaining safe distances from both their platoon predecessor and road boundaries, provided the initial conditions are safe. The effectiveness of the proposed approach is demonstrated through theoretical analysis, simulation studies, and experimental validation using connected miniature vehicles.

The rest of the paper is structured as follows. Section II provides preliminary results about Constructive barrier feedback. In Section III, we define the platoon formation problem and present the vehicle model used for control design in this study. Section IV outlines the formulation of the proposed method. The stability property of the method is further stated in Section V. Section VI presents simulation results aimed at validating the effectiveness of the proposed method. Additionally, we compare these results with a baseline, represented by the nominal control without the constructive barrier feedback component. Experimental studies based on miniature vehicles are conducted and presented in Section VII. Finally, concluding remarks and insights for future research are summarized in Section VIII.

II. PRELIMINARY

A. Constructive barrier feedback for collision avoidance

In this section, we will recall the concept of constructive barrier feedback proposed in [12] for collision avoidance of a leader-follower structure in which each agent dynamics is described as a double integrator as follows

$$\begin{cases} \dot{\mathbf{p}}_i = \mathbf{v}_i \\ \dot{\mathbf{v}}_i = \mathbf{u}_i \end{cases} \quad (1)$$

where $\mathbf{p}_i \in \mathbb{R}^m (m \geq 2)$ is the position, $\mathbf{v}_i \in \mathbb{R}^m$ is the velocity of each agent i , respectively, and $\mathbf{u}_i \in \mathbb{R}^m$ is the input acceleration.

To get an effective reactive collision avoidance without affecting the stability property of the nominal controller, feedback controller u_i is designed in [12] as:

$$\mathbf{u}_i = \mathbf{u}_i^n + \mathbf{u}_i^c, \quad (2)$$

where \mathbf{u}_i^n is the nominal control input ensuring the asymptotic (or the exponential) convergence of the states $(\mathbf{p}_i, \mathbf{v}_i)$ to the desired trajectory. \mathbf{u}_i^c , is a dissipative *control barrier feedback* slowing down the relative velocity of agent i in the direction of the neighbor agent j , $\mathbf{g}_{ij} := \frac{\mathbf{p}_i - \mathbf{p}_j}{\|\mathbf{p}_i - \mathbf{p}_j\|}$, without

compromising the stability nature of the nominal control action

$$\mathbf{u}_i^c = \mathbf{g}_{ij} \frac{\dot{d}_{ij}}{d_{ij}} \quad (3)$$

where $d_{ij} := \|\mathbf{p}_i - \mathbf{p}_j\| - r$ and the divergent flow $\frac{\dot{d}_{ij}}{d_{ij}}$ can be obtained directly from the optical flow using visual information [15], or estimated from the measure of d_{ij} [16].

To illustrate the obstacle avoidance principle employed in this context, let's consider a 2-agent system. Using the above definitions of $d = d_{ij}$ and $\dot{d} = \dot{d}_{ij} = \mathbf{g}_{ij}^\top (\mathbf{v}_i - \mathbf{v}_j)$, it is straightforward to verify that:

$$\ddot{d} = -k_o \frac{\dot{d}}{d} - \alpha_i(t) \quad (4)$$

with $\alpha_i(t) = -\frac{\|\pi_{\mathbf{g}_{ij}}(\mathbf{v}_i - \mathbf{v}_j)\|^2}{d+r} - \mathbf{g}_{ij}^\top (\mathbf{u}_i - \mathbf{u}_j)$. The barrier effect of \mathbf{u}_i^c , is announced in the following technical lemma:

Lemma 1: Given the dynamics (4) with k_o a positive gain and $\alpha_i(t)$ a continuous and bounded function. Then for any initial condition satisfying $d(0) > 0$ and $\phi(0) = \frac{\dot{d}(0)}{d(0)}$ bounded, the following assertions hold:

- 1) d remains positive, $\forall t \geq 0$.
- 2) d converges to zero as $t \rightarrow \infty$ if and only if $\lim_{t \rightarrow \infty} \int_0^t \alpha(\tau) d\tau \rightarrow +\infty$.
- 3) If d converges to zero, then \dot{d} is bounded and converges to zero, and $\phi(t)$ remains bounded, $\forall t \geq 0$. Furthermore, if $\alpha_i(t)$ converges to a positive constant $\alpha^0 > \epsilon > 0$, then $\frac{\dot{d}}{d} \rightarrow -\frac{\alpha^0}{k_o}$ and hence \ddot{d} converges to zero.

Proof of the lemma is given in [12]. This lemma shows the safety invariance property, such that, as long as the initial distance $d(0)$ is positive, d will never cross zero for all times as long as the nominal controller \mathbf{u}_i^n , the neighboring agent input \mathbf{u}_j , and the relative velocity $\mathbf{v}_i - \mathbf{v}_j$ are continuous and bounded.

III. PROBLEM FORMULATION

This paper considers a platoon formation tracking control problem for n vehicles on a curved multi-lane road. The concept of constructive barrier feedback is exploited in the control design to ensure collision avoidance between neighboring vehicles and the road edges during the platoon formation process. Each vehicle in the platoon is assumed to be connected to its neighboring agents under a directed graph topology as described in the following assumption:

Assumption 1: The topology \mathcal{G} is fixed and described by an acyclic digraph with a single directed spanning tree, as shown in Fig. 1. Without loss of generality, agents are numbered (or can be renumbered) such that agent 1 is the leader, i.e., $\mathcal{N}_1 = \emptyset$, all other agents i , $i \geq 2$ are followers whose neighboring set is $\mathcal{N}_i = \{i-1\}$.

For vehicle dynamics, instead of a simple second-order integrator model considered as in the previous work [12], the motion of each vehicle i is described by a nonholonomic

second-order kinematic bicycle model

$$\begin{cases} \dot{p}_{xi} = v_i \cos \theta_i \\ \dot{p}_{yi} = v_i \sin \theta_i \\ \dot{v}_i = a_i \\ \dot{\theta}_i = v_i \chi_i \end{cases} \quad (5)$$

where $\mathbf{p}_i = [p_{xi} \ p_{yi}]^\top \in \mathbb{R}^2$ is the center position of the rear axle for vehicle i expressed in a common fixed world frame \mathcal{I} . θ_i and v_i indicate the orientation and speed of vehicle i , respectively. The control input are acceleration a_i and input curvature $\chi_i = \frac{\tan \delta_i}{L_i}$, where δ_i and L_i denote steering angle and wheel base of vehicle i .

The platoon formation tracking control on a curved road can be considered a combination of path-following and formation-control problems. The control design strategy, hence, can be decoupled as i) designing lateral control laws for follower vehicles, ensuring a geometrical convergence towards the reference path regardless of the translational velocity v_i ; ii) deriving longitudinal control laws for the follower vehicles to achieve desired relative arc length with its neighboring vehicle on the reference path while maintaining the same desired speed as its neighboring vehicle $i - 1$.

To conveniently handle the vehicle control problem along the given reference path, we transform the expression of the vehicle dynamics from the fixed world frame \mathcal{I} to a reference frame aligned with the path \mathcal{F}_i similarly to the path following control problems in [17]. The path-aligned frame is analogous to the Frenet frame with the distinction that the normal direction of the path is not necessarily oriented toward the path's curve. It can be seen as a kinematically equivalent fictitious vehicle's virtual frame on the path with longitudinal and lateral axes $\boldsymbol{\rho}_i$ and $\boldsymbol{\eta}_i$, respectively, as shown in Fig. 2. Since the virtual vehicle i is defined by the orthogonal projection of the actual vehicle i 's position onto the reference path, using the result from [17], the velocity of the virtual vehicle satisfies the following condition

$$v_i^r = \frac{v_i \cos \tilde{\theta}_i}{1 - \chi_i^r \tilde{y}_i} \quad (6)$$

where \tilde{y}_i and $\tilde{\theta}_i = \theta_i - \theta_i^r$ denote the lateral displacement error and orientation error of vehicle i with respect to the virtual frame \mathcal{F}_i with following dynamics

$$\begin{cases} \dot{\tilde{y}}_i = v_i \sin \tilde{\theta}_i \\ \dot{\tilde{\theta}}_i = v_i \left(\chi_i - \frac{\chi_i^r \cos \tilde{\theta}_i}{1 - \chi_i^r \tilde{y}_i} \right) \end{cases} \quad (7)$$

where χ_i^r is curvature of the virtual vehicle i on reference path. The curvature χ_i is the control input to be designed as the lateral controller to drive $(\tilde{y}_i, \tilde{\theta}_i)$ to zero. Note that equation (6) and (7) are well defined as long as the projection onto the path is unique, that is $|\tilde{y}_i| < \frac{1}{\chi_i^r}$.

Note that in the classical path-following problem, translational and orientation control are typically decoupled to stabilize the equilibrium $(\tilde{y}, \tilde{\theta}) = (0, 0)$ independently from

the translational motion. In the proposed approach, longitudinal control is an additional objective aimed at tracking the preceding vehicle. In this context and in contrast to the path-following literature, we reverse the constraint in (6) by first imposing the desired dynamics of the virtual vehicle v_i^r and then use this constraint to determine the control action for the actual vehicle:

$$v_i = v_i^r \frac{1 - \chi_i^r \tilde{y}_i}{\cos \tilde{\theta}_i} \quad (8)$$

The reversed constraint is well-defined given $|\tilde{\theta}_i| < \frac{\pi}{2}$. Hence, the design strategy focuses first on the virtual acceleration control input for the virtual follower vehicle i . Analyze the dynamics of arc length and velocity (s_i, v_i^r) of the virtual vehicle i ,

$$\begin{cases} \dot{s}_i = v_i^r \\ \dot{v}_i^r = a_i^r \end{cases} \quad (9)$$

where a_i^r is the virtual acceleration control to be designed to drive (s_i, v_i^r) to the desired arc length and velocity (s_i^*, v_i^*) . Note that as long as the constraints $|\tilde{y}_i| < \frac{1}{\chi_i^r}$ and $|\tilde{\theta}_i| < \frac{\pi}{2}$ associated with equations (6) and (8) are fulfilled respectively, one can recover the actual input a_i from a_i^r , χ_i , the state variables $(v_i, \tilde{\theta}_i, \tilde{y}_i)$ and the reference path information $(\chi_i^r, \dot{\chi}_i^r)$ using the derivative of (8):

$$a_i = \frac{1}{\cos \tilde{\theta}_i} \left(a_i^r (1 - \chi_i^r \tilde{y}_i) + v_i \sin \tilde{\theta}_i \dot{\tilde{\theta}}_i - v_i^r (\dot{\chi}_i^r \tilde{y}_i + \chi_i^r \dot{\tilde{y}}_i) \right) \quad (10)$$

Now, since for any continuous function $f(t)$ and $g(t)$ having $\dot{f}(t) = \dot{g}(t)$ does not imply that $f(t) = g(t)$, one suggests the following modification to satisfy the constraint (8) :

$$a_i = \frac{1}{\cos \tilde{\theta}_i} \left(a_i^r (1 - \chi_i^r \tilde{y}_i) + v_i \sin \tilde{\theta}_i \dot{\tilde{\theta}}_i - v_i^r (\dot{\chi}_i^r \tilde{y}_i + \chi_i^r \dot{\tilde{y}}_i) \right) - k \left(v_i^r \frac{1 - \chi_i^r \tilde{y}_i}{\cos \tilde{\theta}_i} - v_i \right) \quad (11)$$

with k a positive real number.

With the above description, the desired platoon formation is defined as follows (see Fig. 3):

Assumption 2: The leader vehicle, agent 1, is independently controlled such that it is already in its desired configuration: $\tilde{y}_1 = 0$, $\tilde{\theta}_1 = 0$, $v_1 = v_1^* = v^* > 0$, and $s_1 = s_1^*$. The desired configuration of the follower vehicle i , $i \geq 2$ is on the reference path (i.e., $\tilde{y}_i = 0$ and $\tilde{\theta}_i = 0$) while following its platoon predecessor $i - 1$ with desired velocity $v_i^* = v_{i-1}^* > 0$ and desired relative arc length $e_i^* := s_{i-1}^* - s_i^* > L_i + \epsilon > 0$, where $\epsilon > 0$ is a predefined safe margin.

Besides achieving the desired platoon formation, the group of vehicles has to follow the traffic rules and, hence, should not cross the road boundaries. The assumption below is to describe the road environment and its relationship with the reference path.

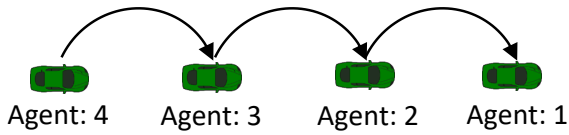


Fig. 1: Interaction topology for a 4-agent platoon formation scenario. The arrow indicates the information access for each agent i from its neighboring agent $i - 1$.

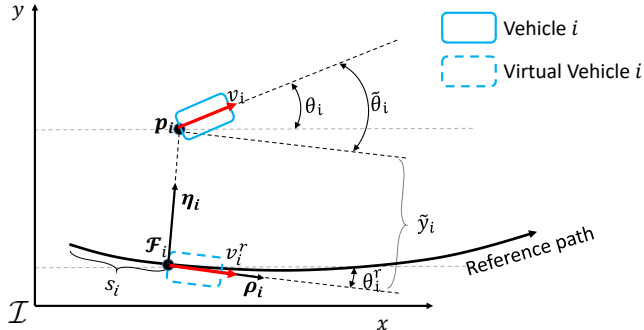


Fig. 2: Kinematic bicycle model for 2-dimensional vehicle motion in both global and Frenet frame. The rectangle of the solid blue line indicates the actual vehicle i and the rectangle of the dashed blue line represents the corresponding virtual vehicle on the path.

Assumption 3: The reference path is parameterized by a smooth arc length s such that the curvature of the path $\chi^r(s)$ is continuous and differentiable with respect to s . Without loss of generality, the platoon's reference path coincides with the road's center line. As shown in Fig. 4, The left and right road edges are parallel to the road center line with a constant lateral width offset distance w such that $\frac{1}{\chi^r} > w > \epsilon_w > 0$ for all s , where $\epsilon_w > 0$ is a predefined lateral safe margin. In addition, for any two distinct points \mathbf{p}_i and \mathbf{p}_j projecting to the reference path with arc length s_i and s_j , $|s_i - s_j| > \epsilon > 0$ implies $\|\mathbf{p}_i - \mathbf{p}_j\|_2 > \epsilon > 0$

The following last assumption assigns the order of the vehicles' index according to their initial arc length projecting on the reference path. This condition will be used later for collision avoidance control design between neighboring vehicles.

Assumption 4: Provided $s_i(0) - s_j(0) \neq 0, \forall i, j \in \mathcal{V} = 1, 2, \dots, n$, the vertex set of n -vehicle system is assigned such that $s_{i-1}(0) - s_i(0) > 0, \forall i \geq 2$.

Given the above ingredients, the safe platoon formation tracking control problem is formally formulated as follows:

Problem 1: Under Assumptions 1 - 4, design lateral and longitudinal controller χ_i and a_i^r , respectively for follower vehicles $i \geq 2$, under which the multi-vehicle system achieves the desired platoon formation described in Assumption 2 while guaranteeing collision-free to road edges and between neighboring vehicles for all the time

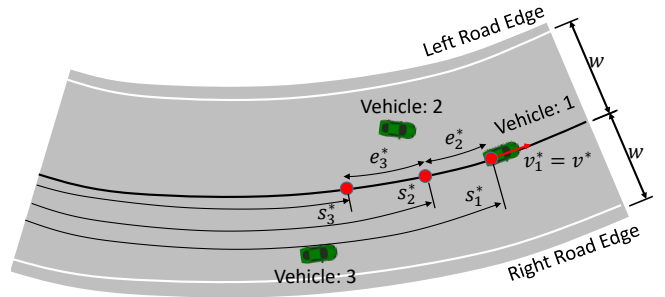


Fig. 3: Road layout to illustrate the desired platoon formation.

IV. SAFE PLATOONING AND MERGING CONTROLLER DESIGN

A. Lateral controller design

From the previous problem formulation in Section III, the lateral control design aims to ensure the follower vehicle a geometrical convergence towards the reference path while guaranteeing collision-free with the road edges. Inspired by the work [12], the safe lateral controller for each follower vehicle $i \geq 2$ is proposed as two parts:

$$\chi_i = \chi_i^n + \chi_i^c \quad (12)$$

where χ_i^n is the nominal controller that ensures the stabilization of the origin of error variable $(\tilde{y}_i, \tilde{\theta}_i)$ and χ_i^c is the constructive barrier feedback to be designed for avoiding collision with the road edges.

Hence, the nominal lateral controller for the follower vehicle $i \geq 2$ is designed as

$$\chi_i^n = -k_1 \frac{\sin \tilde{\theta}_i}{\tilde{\theta}_i} \tilde{y}_i - k_2 \text{sign}(v_i) \tilde{\theta}_i + \frac{\chi_i^r \cos \tilde{\theta}_i}{1 - \chi_i^r \tilde{y}_i} \quad (13)$$

where k_1 and k_2 are positive gains, the first two terms are designed to correct lateral error \tilde{y}_i and orientation error $\tilde{\theta}_i$ respectively, and the last is the feedforward term used to track the reference curvature χ_i^r .

To prevent vehicles from crossing the road edges, we define the lateral safety distance to the left and right road edges, respectively, as

$$d_i^{\eta L} = w - \tilde{y}_i - \epsilon_w, \quad d_i^{\eta R} = w + \tilde{y}_i - \epsilon_w \quad (14)$$

where w is the distance to the road edge from the reference path and $\epsilon_w > 0$ is a predefined safe margin as seen in Fig. 4.

It is straightforward to verify that $d_i^{\eta L} > 0$ and $d_i^{\eta R} > 0$ implies that i) vehicle i stays within the left and right road edges with a predefined safety margin $\epsilon_w > 0$, ii) $|\tilde{y}_i| < w - \epsilon_w < \frac{1}{|\chi_i^r|}$, based on Assumption 3, which ensures that v_i^r in (6) is well defined.

Analogous to the divergent flow used in (3), the lateral constructive barrier feedback χ_i^c is designed as:

$$\chi_i^c = -k_3 \left(\frac{d_i^{\eta R \prime}}{d_i^{\eta R}} - \frac{d_i^{\eta L \prime}}{d_i^{\eta L}} \right) \quad (15)$$

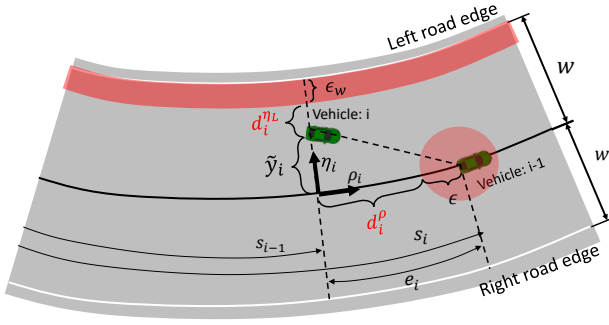


Fig. 4: The lateral safety distance d_i^{nL} of vehicle i with respect to road edges and the longitudinal safety distance d_i^p of vehicle i with respect to its predecessor $i - 1$.

where the notation $(\cdot)'$ denotes derivative with respect to the curvilinear abscissa $\sigma = \int_0^t |v_i(\tau)| d\tau$, i.e., $d_i^{nL}' = \frac{d}{d\sigma} d_i^{nL} = -\text{sign}(v_i) \sin \tilde{\theta}_i$ and $d_i^p' = \text{sign}(v_i) \sin \tilde{\theta}_i$. Hence χ_i^c can be represented as

$$\chi_i^c = -k_3 \left(\frac{1}{d_i^{nL}} + \frac{1}{d_i^{nR}} \right) \text{sign}(v_i) \sin \tilde{\theta}_i \quad (16)$$

Instead of using the time derivative of the distance as in [12], the innovation here is to use the derivative of the distance with respect to the new variable σ to avoid longitudinal translational velocity v_i appearing in the divergent flow, decoupling the lateral and longitudinal control design.

B. Longitudinal controller design

For the longitudinal control, the design is initiated over the virtual vehicle. The virtual acceleration control input a_i^r in (9) is designed as two parts similar to the lateral controller (12)

$$a_i^r = a_i^n + a_i^c. \quad (17)$$

The nominal controller a_i^n is responsible for driving the virtual vehicle's longitudinal state (s_i, v_i^r) toward the desired platoon configuration (s_i^*, v_i^*) . It is defined as

$$a_i^n = k_4 \tilde{e}_i + k_5 \nu_i + a_{i-1}^r \quad (18)$$

where $\tilde{e}_i := e_i - e_i^*$ represents the relative longitudinal position error, with $e_i = s_{i-1} - s_i$ denoting the difference in arc length between virtual agent i and $i-1$. The desired inter-vehicle spacing is given by e_i^* . The term $\nu_i := (v_{i-1}^r - v_i^r)$ is the relative velocity error, and k_4 and k_5 are positive gains.

To prevent collision between vehicle i and $i - 1$, the longitudinal safety distance d_i^p between virtual vehicles i and $i - 1$ is introduced as

$$d_i^p := e_i - \epsilon \quad (19)$$

where $\epsilon > 0$ is the safety margin. See Fig. 4 for a graphic view of the safety distance. Recall Assumption 3, one concludes that collision-free between actual vehicles i and $i-1$ is guaranteed, i.e., $\|\mathbf{p}_{i-1} - \mathbf{p}_i\|_2 > \epsilon > 0$, as long as the collision-free between virtual vehicles holds, i.e., $d_i^p > 0$.

Finally, the longitudinal constructive barrier feedback for collision avoidance between neighboring virtual vehicles is designed as

$$a_i^c = k_6 \frac{\dot{d}_i^p}{d_i^p} \quad (20)$$

where $\dot{d}_i^p = \nu_i$, and k_6 is a positive control gain.

V. STABILITY ANALYSIS

Under the proposed control design, the following lemma shows safety guarantees and equilibrium analysis of the longitudinal controller.

Lemma 2: Consider a n -vehicle system with the system dynamic (5) and the virtual longitudinal control (17), (18) and (20). If Assumption 1 - 4 are satisfied, then for any bounded initial conditions such that $d_i^p(0) > 0$ and $a_i^c(0)$ bounded, the following assertions hold $\forall i \in \mathcal{V}/\{1\}, \forall t \geq 0$:

- 1) vehicle i remains collision-free with its neighboring vehicle $i - 1$, i.e., $d_i^p(t)$ remains positive, and the controller a_i^r is well-defined and bounded;
- 2) the origin of (\tilde{e}_i, ν_i) is asymptotically stable;

The proof of this lemma is provided in Appendix A.

Under both lateral and longitudinal controllers, the multi-vehicle systems' safety invariant properties and stability analysis are provided by the following theorem.

Theorem 1: Consider a n -vehicle system with the dynamics (5) along with the longitudinal controller defined by (11), (17), (18) and (20) and lateral controller (12), (13) and (16). If Assumption 1 - 4 are satisfied, then under any bounded initial condition satisfying, $d_i^p(0) > 0$, $d_i^n(0) > 0$, $k_1 \tilde{y}_i^2(0) + \tilde{\theta}_i^2(0) < (\frac{\pi}{2} - \epsilon_1)^2$, (with $\epsilon_1 \ll 1$ a positive number), $a_i^c(0)$ and $\chi_i^c(0)$ bounded, the following assertions hold $\forall i \in \mathcal{V}/\{1\}, \forall t \geq 0$:

- 1) $|\tilde{\theta}_i| < \frac{\pi}{2}$ and $|\tilde{y}_i| < \frac{1}{\chi_i^c}$, and the n -vehicle system remains safe, i.e., $d_i^p(t)$, $d_i^{nL}(t)$ and $d_i^{nR}(t)$ remain positive;
- 2) the control law χ_i and a_i are well-defined and bounded;
- 3) the origins of $(\tilde{y}_i, \tilde{\theta}_i)$ and $(\tilde{s}_i, \tilde{v}_i) := (s_i - s_i^*, v_i - v_i^*)$ are asymptotically stable;

The proof of this theorem is provided in Appendix B.

VI. SIMULATION RESULTS

To demonstrate the performance of the proposed control method, we design a multilane highway scenario where the shape of the road is generated using the Matlab built-in function *referencePathfrenet()* with fixed waypoints. In particular, a performance comparison between the proposed safe platoon controller (12), (13), (16), (17), (18), and (20), and the nominal platoon controller (13) and (18) (which serves as a baseline control strategy) is provided to emphasize that collision avoidance is ensured without affecting the nominal control objectives. The simulation study is performed for a platoon of five vehicles with two different initial settings, constituting two test scenarios referred to as scenario (A) and scenario (B). The initial conditions are summarized in Table. I and II and is visualized in Fig. 5.

In both scenarios, the controller gains are set as $k_1 = 0.01$, $k_2 = 0.1$, $k_3 = 0.1$, $k_4 = 0.4$, $k_5 = 0.1$, $k_6 = 2$, and the constant parameters are set as $w = 10$ m, $\epsilon_w = 1.2$ m, $\epsilon = 5$ m, $L_i = 4$ m, $e_i^* = 14$ m. $v_i^* = 10$ m s⁻¹.

In scenario (A), the reference path is placed on the road centerline as in Fig. 5a, vehicle states are initiated such that vehicles 1, 3, and 5 are already on the path, while vehicles 2 and 3 are placed to merge into the platoon from the left and right side of the path respectively.

In scenario (B), the reference path is placed parallel to the road centerline with a 2 m offset distance from the left road boundary as in Fig. 5b. Here, vehicles are scattered over the road initially. This setup allows us to evaluate the controller’s performance in steering vehicles from different lanes into the desired platoon formation while demonstrating the capability of the controller to keep vehicles on the road and avoid collisions with each other.

The formation evolution under the proposed control method is shown in Fig. 5, for both scenarios, all vehicles smoothly converge to the desired formation by tracking the reference path and keeping the desired distance with their platoon predecessor. The convergence is more clearly evident in Fig. 6, where the time evolution of the error states \tilde{y}_i , $\tilde{\theta}_i$, \tilde{v}_i , and \tilde{e}_i all converge to zero after approximately 20 seconds for both the proposed controller and the baseline. The simulation results indicate that the convergence property of the baseline controller is preserved by the proposed controller.

The safety can be measured by d_i^p and d_i^n as $d_i^p \leq 0$ and $d_i^n \leq 0$ indicate vehicle-to-vehicle and vehicle-to-road boundary collision (for simplicity of notation here we denote $d_i^n = \min(d_i^{nL}, d_i^{nR})$ for measure of the safety to both sides). As shown in Fig 7 with solid lines, the multi-vehicle system successfully avoids collisions under the proposed controller. In contrast, the multi-vehicle system under the baseline control collides with either neighboring vehicles or the road edges. As shown in Fig. 7a with dashed lines, for scenario (A), the baseline controller failed to keep $d_4^p > 0$, where a collision happened between vehicle 4 and vehicle 3. For scenario (B) as shown in Fig. 7b, the baseline failed to keep $d_2^p > 0$, $d_2^n > 0$, $d_4^p > 0$, $d_4^n > 0$, and $d_5^n > 0$, indicating that vehicles 2, 4, and 5 crossed the road boundary. In addition, vehicle 2 collided with vehicle 1 and vehicle 4 collided with vehicle 3 in scenario (B).

An animation of the simulation results can be found at https://bit.ly/platoon_formation_curved_road., where the performance between the proposed controller and the baseline is compared and visualized. In summary, from the simulation comparisons, one concludes that the proposed safe controller efficiently achieves the nominal formation tracking objective while avoiding collision between neighboring vehicles and road edges with reasonable control inputs.

VII. EXPERIMENTAL RESULTS

This section presents the experimental validation of the proposed methods using connected vehicles. The control

TABLE I: Initial vehicle states for scenario (A)

Vehicle	s_i [m]	\tilde{y}_i [m]	$\tilde{\theta}_i$ [rad]	v_i [m s ⁻¹]
1	50	0	0	10
2	42	4	0	13
3	36	0	0	10
4	28	-4	0	16
5	22	0	0	10

TABLE II: Initial vehicle states for scenario (B)

Vehicle	s_i [m]	\tilde{y}_i [m]	$\tilde{\theta}_i$ [rad]	v_i [m s ⁻¹]
1	50	0	0	10
2	40	-10	0	12
3	29	-2.5	0	10
4	22	-12	0	12
5	12	-5	0	10

algorithms are designed for full-scale autonomous cars with acceleration inputs. However, due to limitations of the available testbed, the experiments were conducted indoors on a fleet of scale-model SVEA vehicles—1:10 scale miniature platforms with velocity control inputs. While the SVEA platforms differ from full-scale cars, they are sufficient to demonstrate the effectiveness of the proposed methods as a proof of concept.

Each SVEA is equipped with a Zed Box powered by an NVIDIA Jetson-embedded computer where the proposed controllers run onboard. Qualisys motion capture system (MOCAP) is used to provide accurate real-time state estimation ($\mathbf{p}_i, v_i, \theta_i$) to each vehicle through communication. Each vehicle i shares its state information (\mathbf{p}_i, v_i) to its neighbor vehicle $i - 1$ according to the communication topology defined in Assumption 1. Both the MOCAP-to-vehicle and vehicle-to-vehicle communication are enabled through a local WiFi network using the ROS framework and a tailored communication protocol. The control algorithms χ_i and a_i are implemented in Python onboard each SVEA with an update frequency fixed at 10 Hz. Since the DC motor on the SVEA platform receives pulse-width modulation (PWM) signals from the electronic speed controller (ESC) to control its shaft speed, the input acceleration a_i is integrated and processed to generate the corresponding PWM signal for accurate speed tracking. The experimental study’s overall control and communication stack is shown in Fig. 9.

The layout of the experiment is shown in Fig. 10. Due to the limitation of lab space, we designed the layout to be a circular-shaped path for continuous driving and testing. As shown in Fig. 10, the red lines indicate the road boundaries, while the blue lines are the reference paths. The reference paths are placed 0.6 meter apart and 0.3 meter away from the left respective right road edges. The vehicles are configured to resemble a platoon merging scenario. Here,

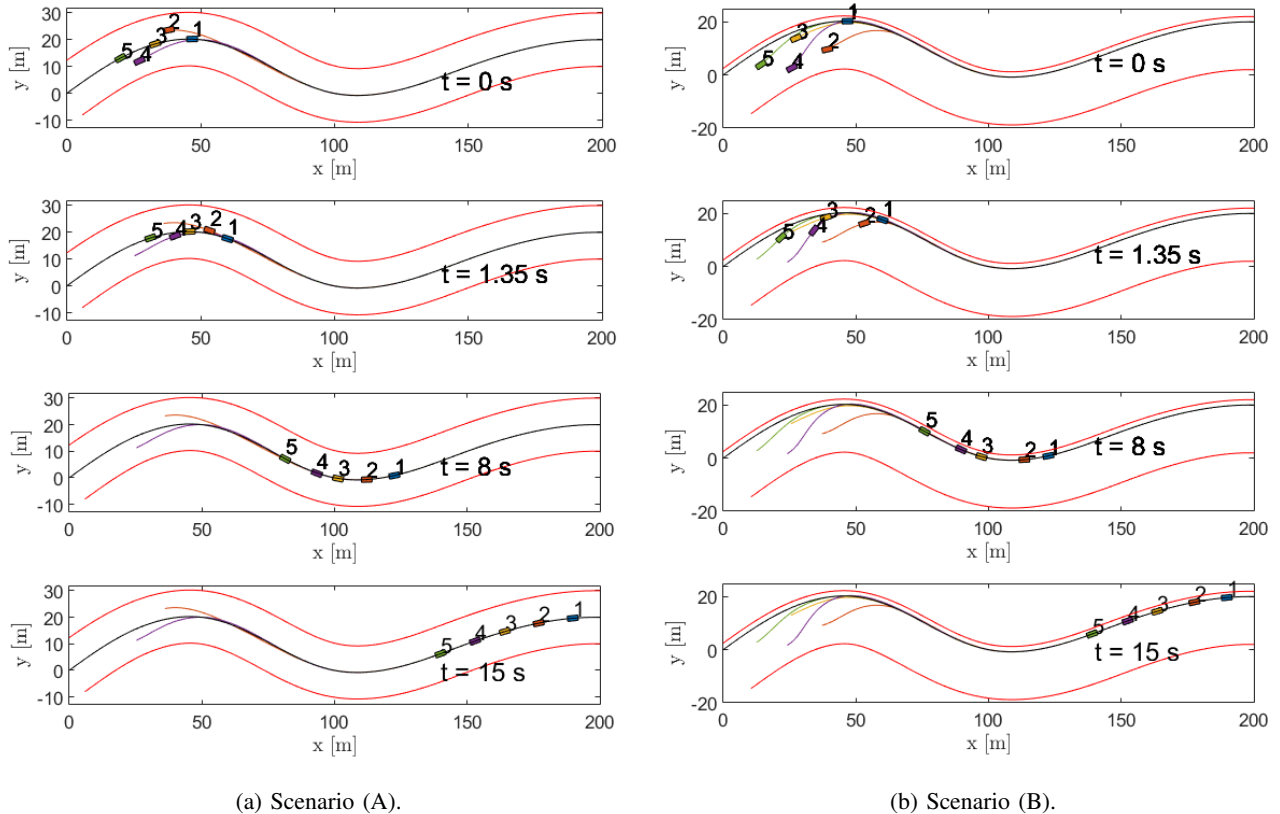


Fig. 5: Time evolution snapshot of the platoon formation process at distinct time points. Two parallel red solid lines are the road edges, the black solid line indicates the desired lane for the platoon, and the color solid lines indicate the vehicle trajectory during the formation process. The left sub-figure shows the result for the merging scenario and the right sub-figure shows the result for the formation scenario.

SVEA 1 and SVEA 3 are designed to drive in a platoon on the inner reference path following a virtual platoon leader simulated onboard SVEA 1, which travels at constant velocity 0.7 m s^{-1} . SVEA 2 is initially placed on the outer reference path with a higher velocity and is designed to merge between the two vehicles given a merging command. The merging command is activated when the longitudinal distance between SVEA 1 and SVEA 2 is less than 0.8 cm .

The controller gains tuned for the experiment scenario are $k_1 = 5$, $k_2 = 2$, $k_3 = 0.5$, $k_4 = 1$, $k_5 = 3$, $k_6 = 0.2$. The desired velocity is $v^* = v_i^* = 0.7 \text{ m s}^{-1}$ and the desired relative arc length $e_i^* = 1.5 \text{ m}$. The wheel base for each vehicle is $L_i = 0.324 \text{ m}$ and the safe margin is chosen as $\epsilon = 0.6 \text{ m}$, $\epsilon_w = 0.15 \text{ m}$. The initial velocity of SVEA 2 before merging the platoon is $v_2(0) = 1.2 \text{ m s}^{-1}$.

To analyze the effectiveness of the proposed method, we again compare the proposed safe platoon controller with the nominal controller as the baseline. The experimental results are presented from the time when the merging command is activated. As shown in Fig. 11, SVEA vehicles' states converge to desired values under both the safe platoon controller and baseline controller. It demonstrates the robustness of the proposed controller under inaccurate actuation of the miniature vehicle. For safety, in Fig. 12a, the proposed

controller guarantees both d_2^p and d_2^n positive, resulting in a safe merging process. In comparison, the baseline controller failed to keep d_2^n above zero as shown in Fig. 12b, resulting in SVEA 2 driving over the road boundary during merging. For longitudinal safety distance d_i^p between vehicles, due to safety, we did not tune the experimental setting to stress test the difference in terms of inter-vehicle safety between the proposed controller and the baseline controller. But the smaller value of d_i^p in Fig. 12b indicates a higher collision risk of the baseline controller. Finally, the input acceleration and steering are shown in Fig. 13. The proposed safe platoon controller and the baseline generate similar input signals with reasonable magnitude.

The experiments are recorded and the video can be found at https://bit.ly/platoon_formation_experiment. In summary, we conclude that the proposed safe platoon controller is applicable in practical implementations.

VIII. CONCLUSION

This study addresses the problem of platoon formation on multi-lane roads with a general curved shape. The controller design is structured into two key components: path-following and longitudinal formation. To ensure safety, a constructive

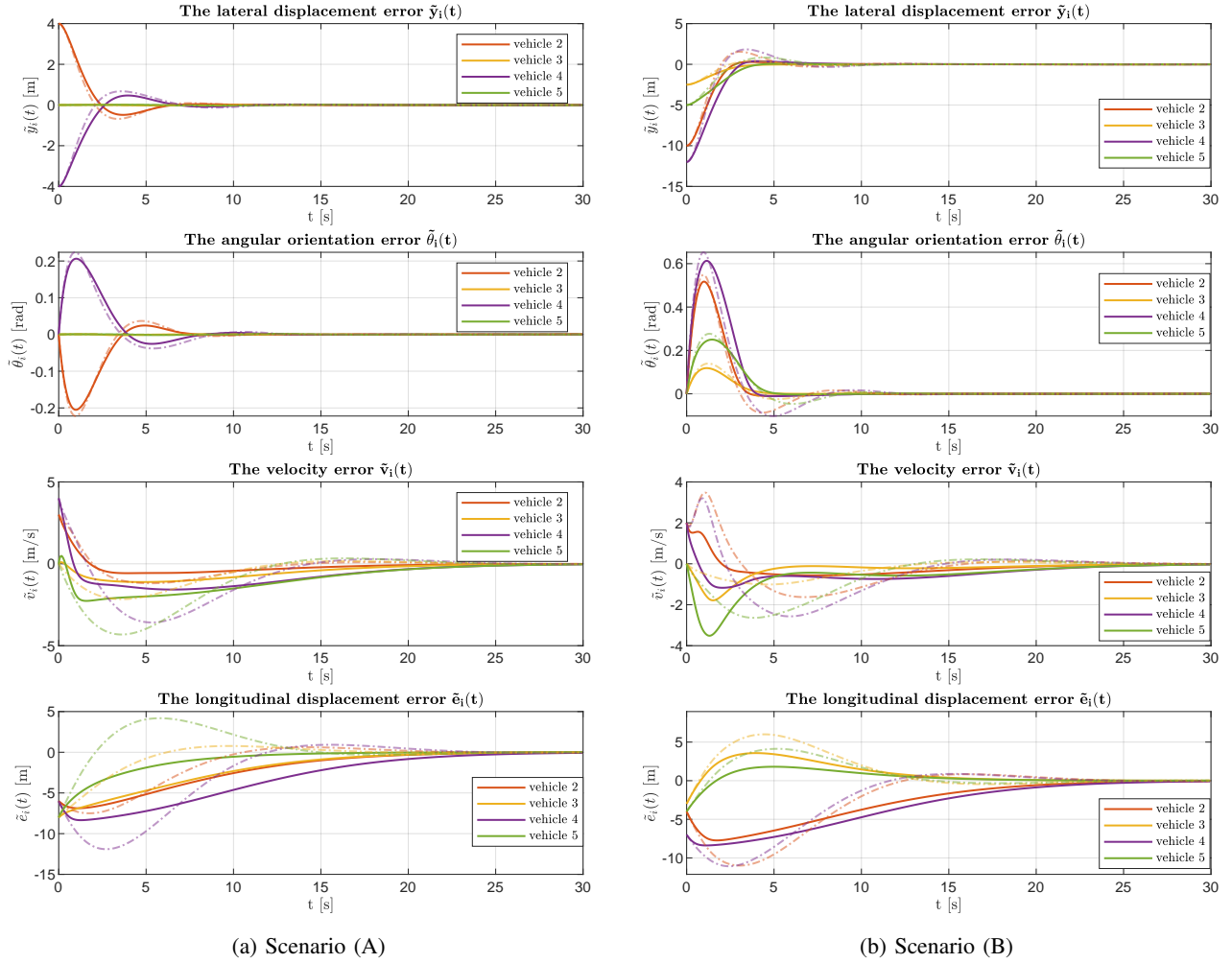


Fig. 6: Time evolution of the lateral displacement error $\tilde{y}_i(t)$, the angular orientation error $\tilde{\theta}_i(t)$, the velocity error $\tilde{v}_i(t)$, and the longitudinal displacement error $\tilde{e}_i(t)$ for all $i = \{2, 3, 4, 5\}$ with respective color-coded lines. The solid lines indicate results under the proposed controller (12), (13), (16), (17), (18), and (20). The transparent dashed lines indicate the result under the baseline controller (13) and (18).

barrier feedback mechanism is introduced for both components, enabling lateral avoidance of road boundaries and longitudinal avoidance of preceding vehicles. Theoretical and numerical analyses are conducted to evaluate the performance and safety properties of the proposed method. Additionally, the method is experimentally validated using miniature vehicles, demonstrating its practical applicability in real-world scenarios.

Future research will focus on enhancing the controller's capabilities by incorporating on-road obstacle avoidance during formation. Furthermore, a deeper analysis of the method's robustness against model uncertainties and measurement errors is essential to further strengthen its reliability in practical implementations.

APPENDIX

A. Proof of Lemma 2

Proof: Recall (9), (17), (18), and (20), the closed-loop dynamics of the state (\tilde{e}_i, ν_i) is expressed as

$$\begin{cases} \dot{\tilde{e}}_i = \nu_i \\ \dot{\nu}_i = -k_4 \tilde{e}_i - k_5 \nu_i - k_6 \frac{d_i^p}{d_i} \end{cases} \quad (21)$$

Consider the following Lyapunov function

$$\mathcal{L}_i = \frac{1}{2} k_4 \tilde{e}_i^2 + \frac{1}{2} \nu_i^2 \quad (22)$$

Recall (21) and use the fact that $\frac{d_i^p}{d_i} = \nu_i$, one has

$$\dot{\mathcal{L}}_i = -k_5 \nu_i^2 - k_6 \frac{\nu_i^2}{d_i} \quad (23)$$

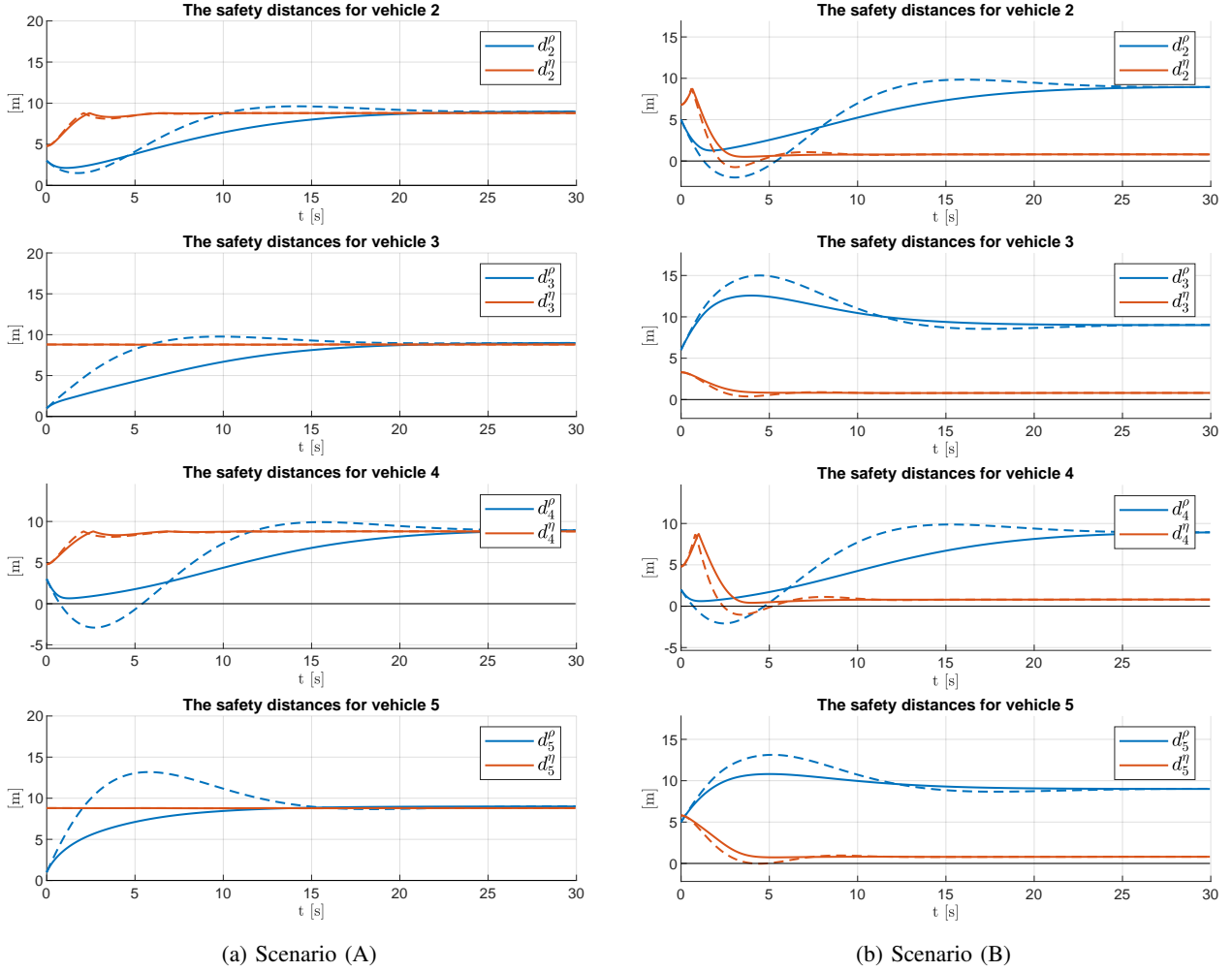


Fig. 7: Time evolution of the safety distance $d_i^p(t)$ and $d_i^n(t)$ for all $i \in \{2, 3, 4, 5\}$. The solid lines indicate the evolution of $d_i^p(t)$ and $d_i^n(t)$ under the proposed controller (12), (13), (16), (17), (18), and (20). The dashed lines indicate the result under the baseline controller (13) and (18).

which is negative semi-definite as long as $d_i^p > 0$. Hence one concludes that (\tilde{e}_i, ν_i) is bounded $\forall t \geq 0$ provided $d_i^p > 0$ for all $t > 0$.

Proof of item (1):

Analyze the derivatives of $\dot{d}_i^p = \nu_i$, one has

$$\ddot{d}_i^p = -k_6 \frac{\dot{d}_i^p}{d_i^p} - k_4 \tilde{e}_i - k_5 \nu_i \quad (24)$$

We will prove that d_i^p remains positive using proof by contradiction. Assume there is a finite time $T > 0$ such that $d_i^p(T)$ approaches zero. Take the integral of (24) from 0 to T , we get

$$k_6 (\ln d_i^p(T) - \ln d_i^p(0)) = \dot{d}_i^p(0) - \dot{d}_i^p(T) - \int_0^T (k_4 \tilde{e}_i + k_5 \nu_i) d\tau \quad (25)$$

The left-hand side of the above equation tends to negative infinity, while the right-hand side is either bounded or tends to positive infinity since \tilde{e}_i and ν_i are bounded for all

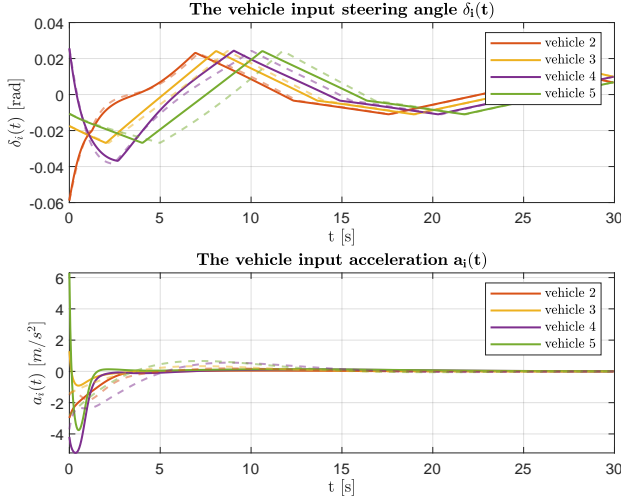
$0 < t < T$, and \dot{d}_i^p is either bounded or negative infinity. This leads to a contradiction, hence, d_i^p remains positive for all time. Therefore, one concludes that (\tilde{e}_i, ν_i) are bounded. From there, direct application of [12, Lemma 2], one ensures that $\frac{\dot{d}_i^p}{d_i^p}$ remains bounded for all the time. This in turn, implies that \dot{a}_i^r (17) is also bounded for all the time.

Proof of item (2):

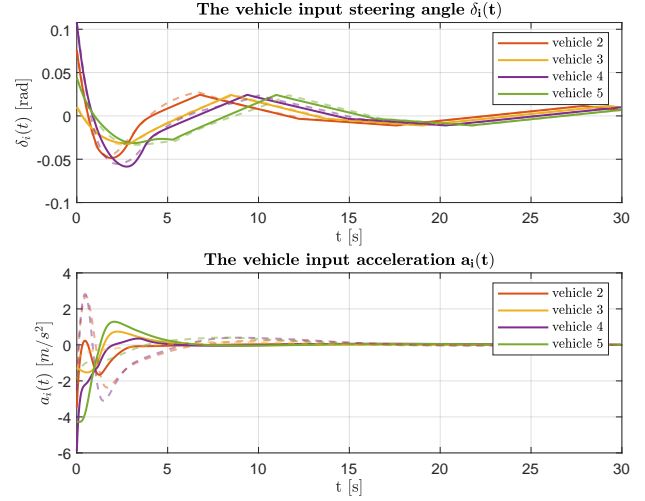
Using a similar argument as the proof of item (2)- [12, Lemma 2] along with Assumption 4, one concludes that the unique equilibrium point $(\tilde{e}_i, \nu_i) = (0, 0)$ is asymptotically stable. ■

B. Proof of theorem 1

Proof: Consider first the lateral error state $(\tilde{y}_i, \tilde{\theta}_i)$, by using (7),(12), (13), and (16), its closed-loop dynamics can



(a) Scenario (A)



(b) Scenario (B)

Fig. 8: The vehicle input acceleration $a_i(t)$ and steering angle $\delta_i(t)$ for all $i = \{2, 3, 4, 5\}$. The solid lines indicate results under the proposed controller (12), (13), (16), (17), (18), and (20). The transparent dashed lines indicate the result under the baseline controller (13) and (18).

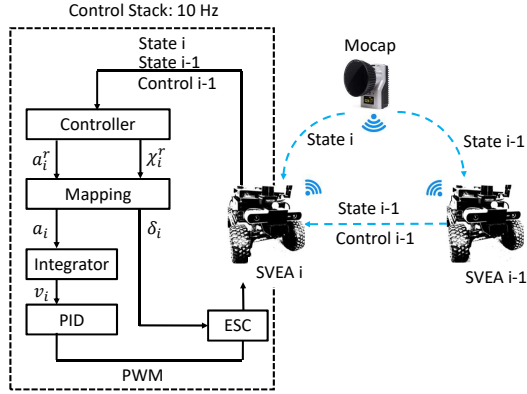


Fig. 9: Control and communication layout of the experimental studies.

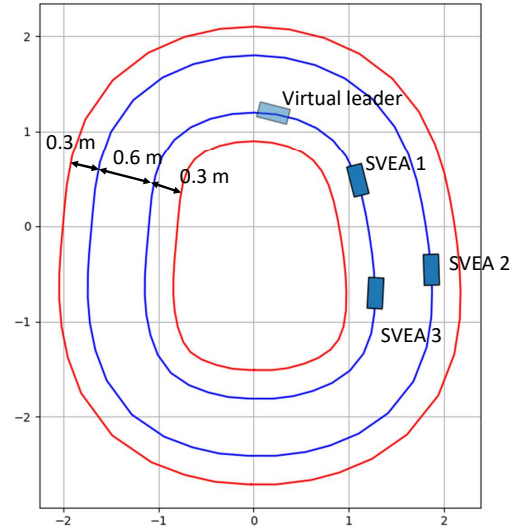


Fig. 10: The platoon merging scenario of 3 SVEAs for the experimental studies.

be expressed as

$$\begin{cases} \dot{\tilde{y}}_i = v_i \sin \tilde{\theta}_i \\ \dot{\tilde{\theta}}_i = -k_1 v_i \tilde{y}_i \frac{\sin \tilde{\theta}_i}{\tilde{\theta}_i} - k_2 |v_i| \tilde{\theta}_i \\ - k_3 |v_i| \left(\frac{1}{d_i^{\eta_L}} + \frac{1}{d_i^{\eta_R}} \right) \sin \tilde{\theta}_i \end{cases} \quad (26)$$

Define the following Lyapunov function:

$$\mathcal{L} = \frac{1}{2} k_1 \tilde{y}_i^2 + \frac{1}{2} \tilde{\theta}_i^2 \quad (27)$$

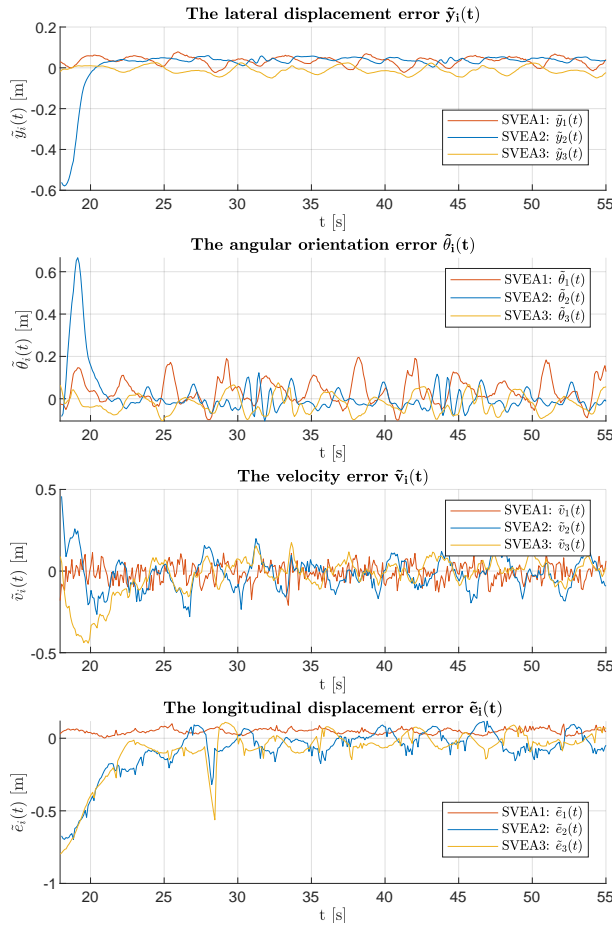
Together with (26), the derivative of (27) is given by:

$$\dot{\mathcal{L}} = -k_2 |v_i| \tilde{\theta}_i^2 - k_3 |v_i| \left(\frac{1}{d_i^{\eta_L}} + \frac{1}{d_i^{\eta_R}} \right) \tilde{\theta}_i \sin \tilde{\theta}_i \quad (28)$$

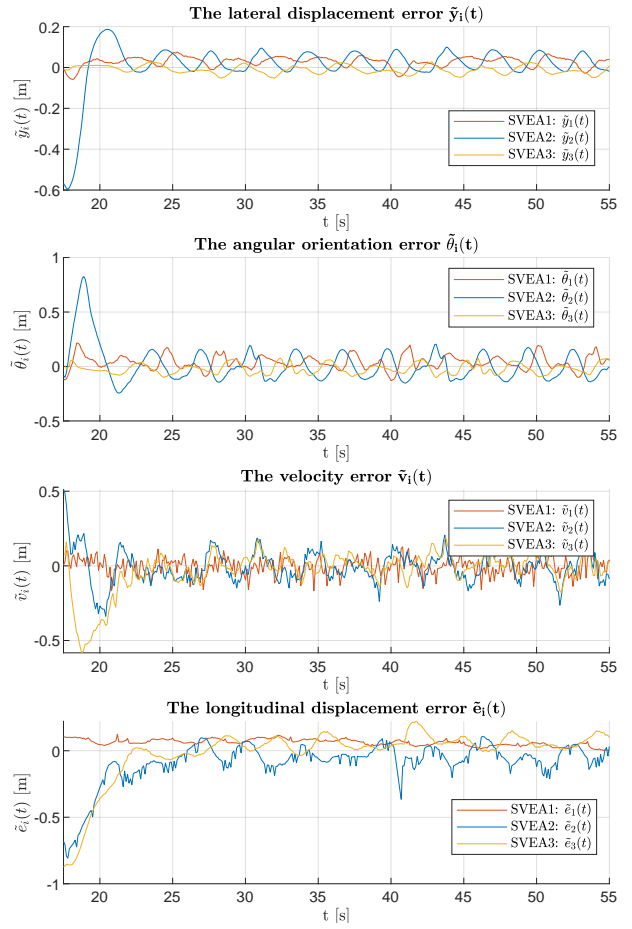
which is negative semi-definite given that $d_i^{\eta_R} > 0$, $d_i^{\eta_L} > 0$, and $|\tilde{\theta}_i| \leq \pi/2 - \epsilon_1$ (and even more so when $|\tilde{\theta}_i| \leq \pi$). One verifies that the state $(\tilde{y}_i, \tilde{\theta}_i)$ is bounded as long as $d_i^{\eta_R} > 0$, and $d_i^{\eta_L} > 0$.

Proof of item (1):

Since Lemma 2- item 1 concludes that d_i^p remains positive all the time. We will focus on showing the bounds of $|\tilde{\theta}_i|$ and $|\tilde{y}_i|$ as well as the positiveness of $d_i^{\eta_L}$ and $d_i^{\eta_R}$. Since the Lyapunov function (27) is nonincreasing, the initial condition $k_1 \tilde{y}_i^2(0) + \tilde{\theta}_i^2(0) < (\frac{\pi}{2} - \epsilon_1)^2$ implies that $|\tilde{\theta}_i(t)| < \pi/2 - \epsilon_1$

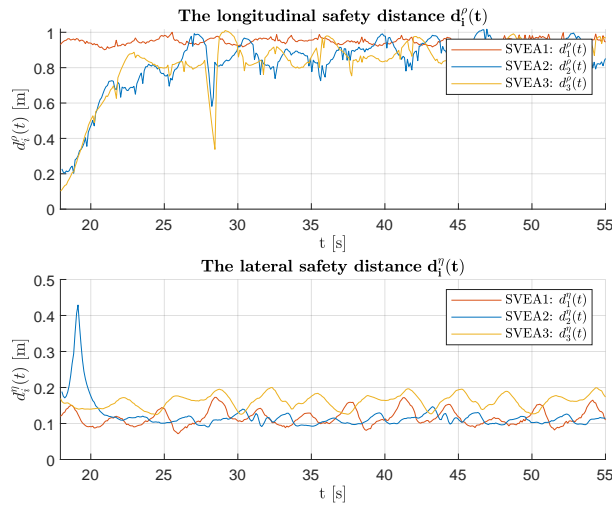


(a) Experiment with the safe platoon controller

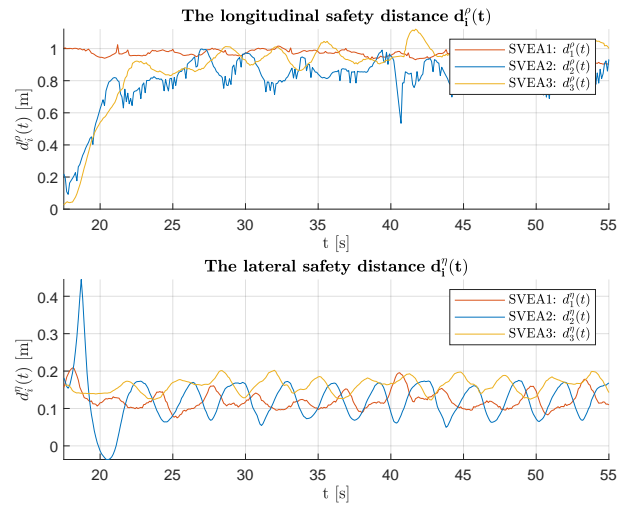


(b) Experiment with the baseline controller

Fig. 11: Time evolution of the lateral position error $\tilde{y}_i(t)$, the angular error $\tilde{\theta}_i(t)$, the velocity error $\tilde{v}_i(t)$, and the relative formation error $\tilde{e}_i(t)$ for SVEA vehicles in the experiment.



(a) Experiment with the safe platoon controller



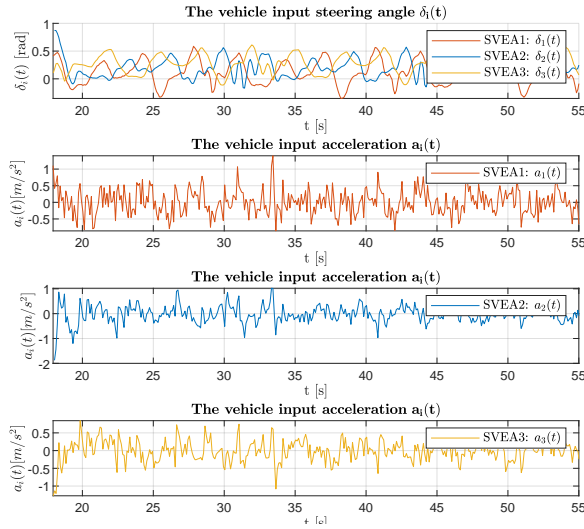
(b) Experiment with the baseline controller

Fig. 12: Time evolution of the safety distance $d_i^l(t)$ and $d_i^r(t)$ for SVEA vehicles in the experiment.

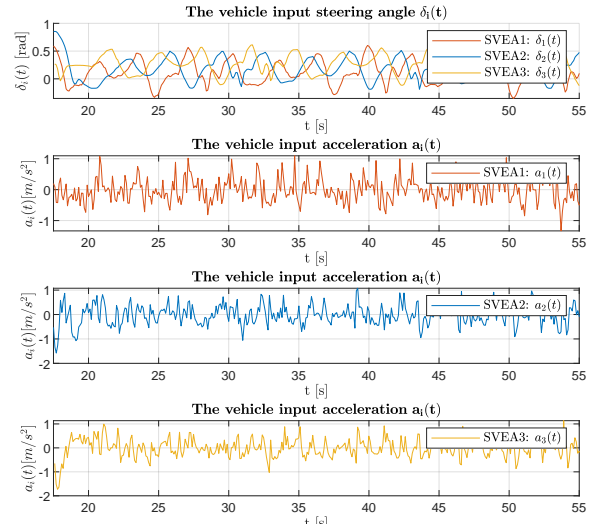
as long $d_i^{\eta L} > 0$ and $d_i^{\eta R} > 0$. Recall that from (14) and Assumption 3, if $d_i^{\eta L} > 0$ and $d_i^{\eta R} > 0$ one ensures that

$$|\tilde{y}_i| < \frac{1}{\chi_i^*}.$$

Due to the convex combination $d_i^{\eta R} + d_i^{\eta L} = 2w - 2\epsilon_w$



(a) Experiment with the safe platoon controller



(b) Experiment with the baseline controller

Fig. 13: The vehicle input acceleration $a_i(t)$ and steering angle $\delta_i(t)$ for SVEA vehicles in the experiment. The input acceleration $a_i(t)$ is displayed in separate plots for clarity.

and the symmetry of the problem at hand, proving $d_i^{\eta R} > 0$ is similar to prove $d_i^{\eta L} > 0$. From now on, we will only show the proof for $d_i^{\eta L}$ and denote $d_i^\eta = d_i^{\eta L}$ for the sake of simplicity. Take the derivative of $d_i^{\eta'} = -\text{sign}(v_i) \sin \tilde{\theta}_i$ with respect to σ to obtain¹:

$$d_i^{\eta''} = -\text{sign}(v_i) \frac{d}{d\sigma} \sin \tilde{\theta}_i \quad (29)$$

since $\frac{d}{d\sigma} \sin \tilde{\theta}_i = \cos \tilde{\theta}_i \text{sign}(v_i) \left(\chi_i - \frac{\chi_i^r \cos \tilde{\theta}_i}{1 - \chi_i^r \tilde{y}_i} \right)$

$$d_i^{\eta''} = -k_3 \cos \tilde{\theta}_i \frac{d_i^{\eta'}}{d_i^\eta} - \alpha_i \quad (30)$$

where

$$\alpha_i(\sigma(t)) = -\cos \tilde{\theta}_i \left(-k_1 \frac{\sin \tilde{\theta}_i}{\tilde{\theta}_i} \tilde{y}_i - k_2 \text{sign}(v_i) \tilde{\theta}_i - k_3 \frac{\text{sign}(v_i) \sin \tilde{\theta}_i}{d_i^{\eta R}} \right)$$

Take integral of the above equation with respect to σ from $\sigma_0 = \sigma(0)$ to $\sigma_T = \sigma(T)$ with a finite σ_T (or equivalently finite T), one has:

$$k_3 \int_{\sigma_0}^{\sigma_T} \cos \tilde{\theta}_i \frac{d_i^{\eta'}}{d_i^\eta} d\sigma = d_i^{\eta'}(\sigma_T) - d_i^{\eta'}(\sigma_0) - \int_{\sigma_0}^{\sigma_T} \alpha_i d\sigma$$

Using the fact that $|\tilde{\theta}| < \frac{\pi}{2}$ in the interval $[\sigma_0, \sigma_T)$, and $\cos \tilde{\theta} > 0$ with a bounded derive, one ensures that there exists $\bar{k}_3 \in (0, k_3]$ a positive and bounded scalar such that $\int_{\sigma_0}^{\sigma_T} k_3 \cos \tilde{\theta}_i \frac{d_i^{\eta'}}{d_i^\eta} d\sigma = \bar{k}_3 \ln \frac{d_i^\eta(\sigma_T)}{d_i^\eta(\sigma_0)}$ and hence:

$$\bar{k}_3 \ln \frac{d_i^\eta(\sigma_T)}{d_i^\eta(\sigma_0)} = d_i^{\eta'}(\sigma_T) - d_i^{\eta'}(\sigma_0) - \int_{\sigma_0}^{\sigma_T} \alpha_i d\sigma \quad (31)$$

¹The derivative of $\text{sign}(v_i)$ with respect to σ is set to zero because when $v_i = 0$ the system is at rest and σ cannot be used as a substitute for time to describe changes.

From this and using the fact that $\frac{d_i^{\eta'}(\sigma_0)}{d_i^\eta(\sigma_0)}$, $d_i^{\eta'}(\sigma_T)$, and $d_i^{\eta'}(\sigma_0)$ are bounded and that α_i is bounded in $[\sigma_0, \sigma_T)$, one concludes that $d_i^{\eta'}$ remains positive by following the same reasoning as in the proof of Lemma 1, Item 1.

Proof of item (2):

Since χ_i^η is bounded because \tilde{y}_i and $\tilde{\theta}_i$ are bounded, to show that controller χ_i is bounded, it suffices to show χ_i^c is bounded when $d_i^{\eta'}$ converges to zero as $\sigma(t)$ tends to infinity. The Proof follows a similar structure of [12, Lemma 2]. We will first show that $d_i^{\eta'}$ converges to zero. Define a new variable μ such that $\mu = \int_{\sigma_0}^{\sigma_t} \frac{1}{d_i^\eta} d\sigma$ and rewrite (30) as

$$\frac{d}{d\mu} d_i^{\eta'} = -k_3 \cos \tilde{\theta}_i d_i^{\eta'} - o(\mu) \quad (32)$$

with $k_3 \cos \tilde{\theta}_i > 0$ and $o(\mu) = d_i^\eta \alpha_i$ a perturbation term that tends to zero when μ goes to infinity (or equivalently when d_i^η converges to zero). One recognizes that this is the dynamics of a first-order system (with $d_i^{\eta'}$ the state) perturbed by a vanishing perturbation. From there, one concludes that $d_i^{\eta'}$ is bounded and also converges to zero as d_i^η converges to zero. To prove that χ_i^c is bounded when $(d_i^{\eta'}, d_i^\eta) \rightarrow (0, 0)$, it suffices to show that $\frac{d_i^{\eta'}}{d_i^\eta}$ is bounded.

Hence, differentiating $\frac{d_i^{\eta'}}{d_i^\eta}$ with respect to μ , one verifies that:

$$\frac{d}{d\mu} \frac{d_i^{\eta'}}{d_i^\eta} = -(k_3 \cos \tilde{\theta}_i + d_i^{\eta'}) \frac{d_i^{\eta'}}{d_i^\eta} - \alpha_i \quad (33)$$

Using the fact that α_i is bounded and $d_i^{\eta'}$ is converging to zero, one ensures that there exists a μ^* or equivalently a σ^* (and therefore a time instant T), such that $(d_i^{\eta'} + k_3 \cos \tilde{\theta}) > 0$, $\forall \mu \geq \mu^*$. From there, one guarantees that $\frac{d_i^{\eta'}}{d_i^\eta}$ is bounded, hence, χ_i is bounded and well-defined for all the time.

To prove a_i is bounded and well-defined, we recall equation (11), (8), and (7). One concludes that a_i is well-defined and bounded since $|\theta_i| < \frac{\pi}{2} - \epsilon_1$, $|\tilde{y}_i| < \frac{1}{\chi_i^r}$, and a_i^r and v_i^r are bounded and well-defined (Lemma 2).

Proof of item (3):

Using Barbalat's Lemma along with a similar argument as the proof of Lemma 2 - item (2) in [12], one concludes that the unique equilibrium point $(\tilde{y}_i, \tilde{\theta}_i) = (0, 0)$ for the lateral subsystem is asymptotically stable.

From Lemma 2 item (2), one concludes that the origin of (\tilde{e}_i, ν_i) is asymptotically stable. Recall equation (6), one has $\tilde{v}_i^r = \tilde{v}_i$ provided $(\tilde{y}_i, \tilde{\theta}_i) = (0, 0)$. From Assumption 2, the leader vehicle is already in its desired states, i.e., $\tilde{s}_1 = 0$ and $\tilde{v}_1 = \tilde{v}_1^r = 0$, hence, the asymptotic stability of $(\tilde{e}_i, \nu_i) = (\tilde{s}_{i-1} - \tilde{s}_i, \tilde{v}_{i-1}^r - \tilde{v}_i^r) = (0, 0)$ and $(\tilde{y}_i, \tilde{\theta}_i) = (0, 0)$ implies that the origin of $(\tilde{s}_i, \tilde{v}_i)$ is also asymptotically stable. ■

REFERENCES

- [1] S. E. Shladover, X.-Y. Lu, B. Song, S. Dickey, C. Nowakowski, A. Howell, F. Bu, D. Marco, H.-S. Tan, and D. Nelson, "Demonstration of automated heavy-duty vehicles," 2006.
- [2] T. Robinson, E. Chan, and E. Coelingh, "Operating platoons on public motorways: An introduction to the sartre platooning programme," in *17th world congress on intelligent transport systems*, vol. 1, 2010, p. 12.
- [3] M. Saeednia and M. Menendez, "Analysis of strategies for truck platooning: Hybrid strategy," *Transportation Research Record*, vol. 2547, no. 1, pp. 41–48, 2016.
- [4] S. Bang and S. Ahn, "Platooning strategy for connected and autonomous vehicles: transition from light traffic," *Transportation Research Record*, vol. 2623, no. 1, pp. 73–81, 2017.
- [5] V. Turri, B. Besselink, and K. H. Johansson, "Cooperative look-ahead control for fuel-efficient and safe heavy-duty vehicle platooning," *IEEE Transactions on Control Systems Technology*, vol. 25, no. 1, pp. 12–28, 2016.
- [6] Y. Zheng, S. E. Li, J. Wang, D. Cao, and K. Li, "Stability and scalability of homogeneous vehicular platoon: Study on the influence of information flow topologies," *IEEE Transactions on intelligent transportation systems*, vol. 17, no. 1, pp. 14–26, 2015.
- [7] L. Xiao and F. Gao, "Practical string stability of platoon of adaptive cruise control vehicles," *IEEE Transactions on intelligent transportation systems*, vol. 12, no. 4, pp. 1184–1194, 2011.
- [8] Y. Li, C. Tang, S. Peeta, and Y. Wang, "Integral-sliding-mode braking control for a connected vehicle platoon: Theory and application," *IEEE Transactions on Industrial Electronics*, vol. 66, no. 6, pp. 4618–4628, 2018.
- [9] I. Karafyllis, D. Theodosis, and M. Papageorgiou, "Lyapunov-based two-dimensional cruise control of autonomous vehicles on lane-free roads," *Automatica*, vol. 145, p. 110517, 2022.
- [10] P. Liu, A. Kurt, and U. Ozguner, "Distributed model predictive control for cooperative and flexible vehicle platooning," *IEEE Transactions on Control Systems Technology*, vol. 27, no. 3, pp. 1115–1128, 2018.
- [11] K. Xu, W. Xiao, and C. G. Cassandras, "Feasibility guaranteed traffic merging control using control barrier functions," in *2022 American Control Conference (ACC)*. IEEE, 2022, pp. 2309–2314.
- [12] Z. Tang, R. Cunha, T. Hamel, and C. Silvestre, "Constructive barrier feedback for collision avoidance in leader-follower formation control," in *2023 62nd IEEE Conference on Decision and Control (CDC)*. IEEE, 2023. [Online]. Available: <https://arxiv.org/abs/2310.14258>
- [13] P. S. Bhagavatula, C. Claudianos, M. R. Ibbotson, and M. V. Srinivasan, "Optic flow cues guide flight in birds," *Current Biology*, vol. 21, no. 21, pp. 1794–1799, 2011.
- [14] X. Chen, Z. Tang, K. H. Johanson, and J. Mårtensson, "Safe platooning and merging control using constructive barrier feedback," in *2024 22nd European Control Conference (ECC)*, 2024.
- [15] L. Rosa, T. Hamel, R. Mahony, and C. Samson, "Optical-flow based strategies for landing vtol uavs in cluttered environments," *IFAC Proceedings Volumes*, vol. 47, no. 3, pp. 3176–3183, 2014.
- [16] M.-D. Hua and H. Rifai, "Obstacle avoidance for teleoperated under-actuated aerial vehicles using telemetric measurements," in *49th IEEE Conference on Decision and Control (CDC)*. IEEE, 2010, pp. 262–267.
- [17] L. Aguilar, T. Hamel, and P. Soueres, "Robust path following control for wheeled robots via sliding mode techniques," in *Proceedings of the 1997 IEEE/RJS International Conference on Intelligent Robot and Systems. Innovative Robotics for Real-World Applications. IROS '97*, vol. 3, 1997, pp. 1389–1395 vol.3.